

Mechanism and First Experimental Demonstration of ILMD-induced Reduction of Intramodal Cross-phase Modulation in Weakly-coupled FMF Transmission

Mingqing Zuo¹, Gang Qiao^{2,3}, Yu Yang³, Chengbin Long², Dawei Ge¹, Dong Wang¹, Yunbo Li¹, Zhangyuan Chen², Dechao Zhang¹, Han Li¹, Juhao Li^{2,3,*}

¹Department of Fundamental Network Technology, China Mobile Research Institute, Beijing 100053, China

²State Key Lab of Advanced Optical Communication Systems and Networks, Peking University, Beijing 100871, China

³Peng Cheng Laboratory, Shenzhen, 518055, China

*juhao_li@pku.edu.cn

Abstract: We for the first time experimentally analyze the interaction between intramodal XPM and ILMD effects in weakly-coupled FMF, and prove that the ILMD could be a major factor for effectively reducing the intramodal XPM impairments. © 2024 The Author(s)

1. Introduction

Recently, weakly-coupled mode-division multiplexed (MDM) transmission adopting linearly-polarized (LP) modes in low-modal-crosstalk few-mode fibers (FMFs) has attracted extensive interests as a candidate to break the capacity bottleneck of fiber-optic transmission systems [1], in which complex intermodal multiple-input-multiple-output (MIMO) digital signal processing (DSP) can be avoided by suppressing all kinds of modal crosstalk over the whole FMF link. Record 1800-km 2-mode (LP₀₁ and LP₀₂) and 525-km 3-mode (LP₀₁, LP₂₁ and LP₀₂) transmission only adopting 2×2 or 4×4 MIMO-DSP have been experimentally demonstrated [2], which for the first time validates the feasibility of long-haul intermodal-free MDM transmission. Accompanying with the modal crosstalk well controlled and the transmission reach greatly increased in state-of-art weakly-coupled MDM systems, the FMF nonlinearity would gradually emerge as a major obstacle preventing the further improvement of system performances, and the understanding of the nonlinear effects in weakly-coupled FMFs and of their influences on system operation become essential for efficient optimization of corresponding MDM systems and accurate assessment of their performances. Of particular interest is the modal dispersion dependence of cross-phase modulation (XPM) especially for the intramodal case. According to previous numerical investigation [3], XPM inside a degenerate LP_{mn} ($m \geq 1, n \geq 1$) mode might be effectively mitigated by intra-LP-mode dispersion (ILMD) among its nonideally-degenerate eigenmodes. However, to the best of our knowledge there has been never been a solid experimental verification for the advantage of ILMD on reducing the intramodal XPM in weakly-coupled FMF transmission.

In this paper, we firstly analyze the impact of the ILMD effect on the intramodal XPM, and then establish an experimental system for evaluating the intramodal XPM impairments in a weakly-coupled 6-LP-mode fiber. The results show that the intramodal XPM noise could be reduced by up to 9.7 dB because of the ILMDs of degenerate LP_{mn} modes, which for the first time verifies that the ILMD could effectively mitigate the intramodal XPM.

2. Mechanism of ILMD-induced intramodal XPM reduction

For a circular-core FMF, the ILMD of degenerate LP modes have been experimentally verified to be tens of times larger than the PMD in SMF or the ILMDs of LP_{0n} modes because of the inherent effective index difference Δn_{eff} among eigenmodes inside each degenerate mode [4]. To further demonstrate the mechanism of the intramodal XPM mitigation induced by ILMD, we take the LP_{mn,ax} mode, one of the four degenerate components, as an example and its optical transmission characteristics through a FMF link under a 2-wavelength-channel modal can be theoretically described as below according to the generalized Manakov equation [5]

$$\frac{\partial u_{1ax}}{\partial z} + j\frac{\beta^{(2)}}{2}\frac{\partial^2 u_{1ax}}{\partial t^2} + \frac{\alpha}{2}u_{1ax} = j\frac{16\gamma}{15}\left[|U_1|^2 u_{1ax} + (|u_{2ax}|^2 + |U_2|^2)u_{1ax} + u_{2ax}u_{2ay}^*u_{1ay} + u_{2ax}u_{2bx}^*u_{1bx} + u_{2ax}u_{2by}^*u_{1by}\right], \quad (1)$$

where u_{1k} and u_{2k} are respectively the slowly-varying complex envelopes of the probe and interfering channels, and k represents different degenerate components i.e. $k = \text{ax}, \text{ay}, \text{bx}$ or by ; $U_{1/2}$ is the generalized Jones vector for the probe or interfering channel consisting of $u_{1/2ax}$, $u_{1/2ay}$, $u_{1/2bx}$, and $u_{1/2by}$; $\beta^{(2)}$ is the chromatic dispersion (CD) coefficient; α is the propagation loss; γ is the nonlinear coefficient. The right side of Eq. (1) indicates the nonlinear impairments, in which the 1st term denotes self-phase modulation (SPM), the 2nd term is for the XPM phase noise, and the 3rd to 5th terms correspond to the XPM crosstalk. With respect to the probe channel, the ILMD causes the

change of relative state of mode (RSOM) by a 4×4 generalized Jones matrix $\mathbf{R} = [\mathbf{R}_1; \mathbf{R}_2; \mathbf{R}_3; \mathbf{R}_4]$ and the interfering signal is rewritten as $\mathbf{U}_2' = \mathbf{R}\mathbf{U}_2$. Here, the driving signal of XPM crosstalk from u_{1ay} is given by

$$u_{2ax}' u_{2ay}^* = \mathbf{R}_1 \mathbf{U}_2 (\mathbf{R}_2 \mathbf{U}_2)^* \quad (2)$$

The driving signal of XPM crosstalk from other components could also be written as similar forms. Moreover, with the change of RSOM, the driving signal of XPM phase noise is expressed as

$$|u_{2ax}'|^2 + |U_2'|^2 = \mathbf{R}_1 \mathbf{U}_2 (\mathbf{R}_1 \mathbf{U}_2)^* + |U_2'|^2 \quad (3)$$

If we divide the FMF into short sections with length equal to the de-correlated length for the probe and interfering channels, \mathbf{R} will be different for each section because of the stochastic nature of ILMD. Thus, the XPM crosstalk of each span is no longer the same and would accumulate in different phases, and for XPM phase noise there would also exist partially random superposition along the FMF transmission, both of which lead to the mitigation of overall XPM impacts. However, it should be noted that the above analysis is carried out when assuming a zero-CD property. With the usual value of CD introduced, the walk-off effect between the probe and interfering channels would break the constructive interference of XPM impairments similarly. In this situation, the ILMD-induced intramodal XPM reduction could still be significant only when the de-correlated length is less than or comparable with the walk-off length of $L_w = T_s/\beta^{(2)}\Delta f$. Because the de-correlated length decreases with the ILMD value [4], it can be expected that the XPM mitigation contributed by ILMD may be observed for degenerate LP_{mn} modes but may be masked by CD-induced walk-off for non-degenerate LP_{0n} modes.

3. Experimental setup and results

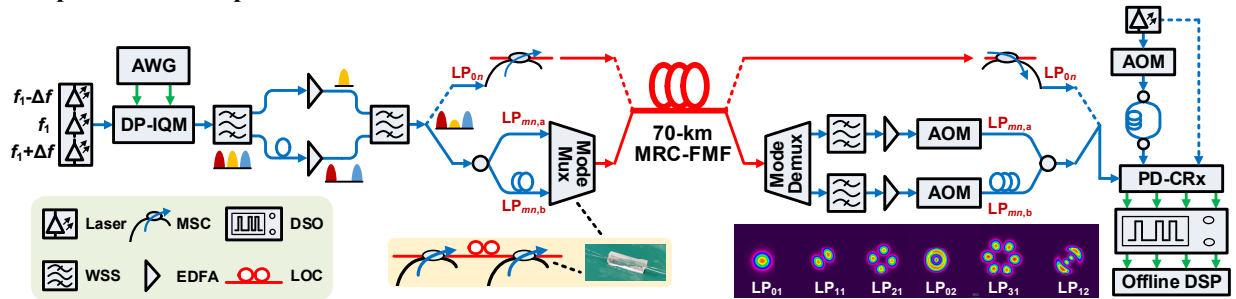


Fig. 1 Experimental setup for evaluating the intramodal XPM distortions in 70-km weakly-coupled 6-LP-mode fiber transmission (insets are the schematic of the cascaded MSCs for LP_{mn} mode conversion and the received modal patterns captured by a coupled-charge camera).

To validate the advantage of ILMD on mitigating the intramodal XPM distortions, we establish an experimental system using a weakly-coupled multiple-ring-core (MRC) 6-LP-mode fiber as shown in Fig. 1. At the transmitter, 3λ signal is generated by a set of external cavity lasers (ECLs, IDPHOTONES CBMA48) coupled by cascaded 50:50 2×1 polarization-maintaining optical couplers (PM-OCs), in which the middle wavelength is the channel under test (CUT) while the others are set as interfering channel bands (ICBs). Then, a 25-GBd 16-ary quadrature amplitude modulation (16QAM) Nyquist baseband signal is generated with a roll-off factor of 0.01 by an arbitrary waveform generator (AWG, Keysight M8199A) operating at 128 GSa/s, which drives a dual-polarization in-phase and quadrature modulator (DP-IQM) to produce DP-16QAM optical signals. Next, the 3λ signal is demultiplexed by a wavelength-selective switch (WSS, Finisar WaveShaper 400A), and the CUT is sent into the upper branch while the ICBs are for the lower branch. After decorrelating with proper delays, the CUT and ICBs are respectively amplified by two erbium-doped fiber amplifiers (EDFAs), and combined by another WSS. For non-degenerate LP_{0n} modes, the signal is directly fed into 70-km FMF for transmission after mode conversion, while for degenerate LP_{mn} modes the signal is evenly split and delayed for two spatial components before FMF transmission. The mode conversion is realized by mode-selective couplers (MSCs) which is fabricated by side-polishing and malting process [6]. To ensure the spatial orthogonality between $LP_{mn,a}$ and $LP_{mn,b}$ modes, a lobe orientation controller (LOC) is inserted between their corresponding MSCs, which is realized by wrapping the fiber around several loops similar to a typical fiber polarization controller [3]. The CUT is launched at -1 dBm/mode and the ICB at 16 dBm/mode. At the receiver, the CUT is filtered and detected by a polarization-diversity coherent receiver (PD-CRx). The received electrical signals are sampled by a real-time digital storage oscilloscope (DSO, Keysight UXR0594AP) operating at 256 GSa/s for performing the offline DSP. For degenerate mode reception, we adopt a time-division multiplexed scheme, in which the optical signals from $LP_{mn,a}$ and $LP_{mn,b}$ modes are temporally separated with a 2-km SMF pigtail and then combined to occupy different time slots, while the same delay is also adopted to the local oscillator for phase

matching. Here, 2×2 MIMO-DSP is used for LP_{01} and LP_{02} modes, and 4×4 MIMO-DSP is for the other LP modes with 4-fold degeneracy.

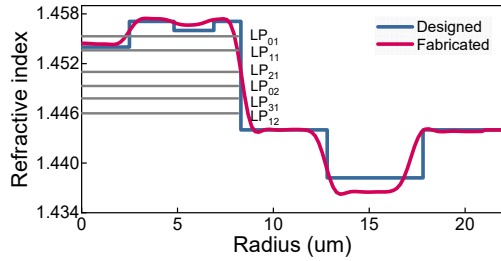


Table 1. Characteristics of each LP mode in fabricated FMF

	LP_{01}	LP_{11}	LP_{21}	LP_{02}	LP_{31}	LP_{12}
PL* (dB/km)	0.215	0.218	0.223	0.228	0.23	0.232
A_{eff} (μm^2)	158	126	134	126	139	133
ILMD ($\text{ps}/\text{km}^{1/2}$)	0.1	5.6	3.7	0.2	4.2	3.3

Fig. 2 Index profile of MRC-FMF and n_{eff} of all 6 LP modes. *PL: propagation loss

Figure 2 shows the index profile of the MRC-FMF and the n_{eff} distribution of all 6 LP modes among which the minimum n_{eff} difference is 1.54×10^{-3} . The characteristics of each LP mode including propagation loss and effective modal area A_{eff} for the fabricated FMF are similar which can be seen in Table 1. Moreover, the ILMD coefficients in the FMF are experimentally measured based on the improved fixed analyzer method (IFAM) [4], in which those of non-degenerate LP_{0n} modes are not larger than $0.2 \text{ ps}/\text{km}^{1/2}$ while those of degenerate LP_{mn} modes range from 3.3 to $5.6 \text{ ps}/\text{km}^{1/2}$. The Q^2 factors after 70-km MRC-FMF transmission for each LP mode are firstly evaluated. It can be observed from Fig. 3(a) that with the frequency spacing Δf between CUT and ICBs decreased, the performances of degenerate LP_{mn} modes with large ILMDs are nearly independent of the frequency spacing especially for LP_{11} mode, while those of LP_{0n} modes degrade significantly due to the emergency of the XPM impacts. Taking LP_{02} mode as an example, the Q^2 factor difference between the cases of $\Delta f = 50 \text{ GHz}$ and 150 GHz has been up to 2.3 dB. To further discuss and compare the intramodal XPM of non-degenerate and degenerate modes, the intramodal XPM intensity with Δf of 50 GHz is calculated by $\sigma_w^2 - \sigma_{w/o}^2$ and presented in Fig. 3(b), in which σ_w^2 and $\sigma_{w/o}^2$ are respectively the noise variance extracted from the recovered constellation diagrams with and without ICBs. To remove the influences of the A_{eff} differences among different LP modes for a fair comparison, the calculated intramodal XPM intensity has been normalized to the same A_{eff} of $130 \mu\text{m}^2$ [3]. We can see that the intramodal XPM noise of non-degenerate LP_{0n} modes are much larger than those of degenerate LP_{mn} modes, in which the maximum difference is 9.7 dB lying between the LP_{01} and LP_{11} modes. The insets of Fig. 3(b) are the corresponding recovered constellation diagrams of LP_{11} and LP_{02} modes, which also indicate severer XPM distortions for the non-degenerate mode.

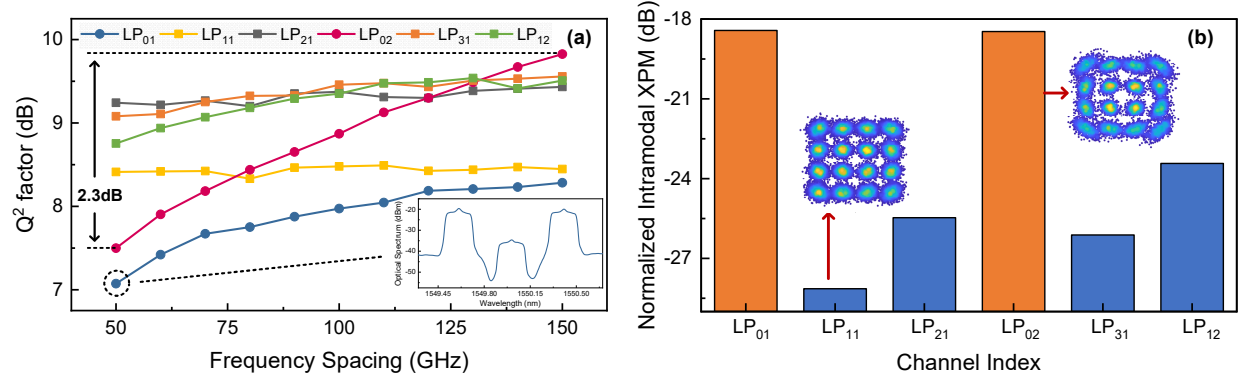


Fig. 3. (a) Q^2 factors of different LP modes versus frequency spacing between CUT and ICBs (inset is the received optical spectrum of LP_{01} mode with Δf of 50 GHz); (b) evaluated normalized intramodal XPM noise power for different LP modes with frequency spacing of 50 GHz.

4. Conclusion

We theoretically investigate the behavior of intramodal XPM distortions including XPM crosstalk and XPM phase noise under ILMD in weakly-coupled FMF, based on which the effective suppression brought by ILMD effect to intramodal XPM is experimentally demonstrated for the first time. This work would be beneficial to the design and performance evaluation of weakly-coupled MDM systems in the future. *This work was supported by National Key Research & Development Program of China (No. 2022YFB2903303)*

5. References

- [1] S. Beppu, et al., JLT, 38(10), 2835-2841, 2020.
- [2] M. Zuo, et al., Opt. Expr., 30(4), 5868-5878, 2022.
- [3] P. Serena, et al., JLT, 40(10), 3263-3276, 2022.
- [4] D. Ge, et al., JLT, 39(22), 7238-7245, 2021.
- [5] A. Mecozzi, et al., Opt. Expr., 20(11), 11673-11678, 2012.
- [6] K. J. Park, et al., Opt. Expr., 24(4), 3543-3549, 2016.